PERGAMON

International Journal of Heat and Mass Transfer 42 (1999) 941–949

International Journal of HEAT and MASS TRANSFER

Large-eddy simulation of the combined convection around a heated rotating cylinder

Rigoberto E. M. Morales, Augusto Balparda, Aristeu Silveira-Neto*

Federal University of Uberlândia, Department of Mechanical Engineering, 38400-206 Uberlândia-MG, Brazil

Received 27 May 1997; in final form 15 April 1998

Abstract

Large-eddy simulation of the combined convection was simulated and the classical results were obtained. The combined convection around the heated rotating cylinder was also simulated and the results agree well with available experimental results. A Nusselt number correlation for the combined convection was proposed. This correlation gives the heat transfer coefficient for the small rotation regime, with an error smaller than 4%. © 1998 Elsevier Science Ltd. All rights reserved.

Nomenclature

C_s Smagorinsky constant
C_p pressure coefficient
$\vec{g}$ gravity acceleration [m s^{-2}]
Gr^* Grashof number ($Gr^* = g\beta R^4 q''/(v^2\kappa)$)
h convection heat transfer coefficient [W m^{-2} °C^{-1}]
$\vec{i}$ unitary vector in the x direction
$\vec{j}$ unitary vector in the y direction
k_s sub-grid scale turbulent kinetic energy [m^2 s^{-2}]
l sub-grid characteristic scale, $l = \sqrt{r\Delta\theta\Delta r}$ [m]
Nu Nusselt number ($Nu = hD/\kappa$)
p pressure [non dimensional]
Pr Prandtl number (v/α)
$\vec{q}$ conductive heat flux [W m^{-2}]
r radial coordinate [non dimensional]
R cylinder radius [m]
Ra^* Rayleigh number ($Ra^* = Gr^*Pr$)
Re Reynolds number ($Re = \omega R^2/v$)
t time [non dimensional]
T temperature [non dimensional]
u radial velocity component [non dimensional]
v tangential velocity component [non dimensional]
S_{ij} deformation tensor [non dimensional].

Greek symbols

α molecular thermal diffusion [m^2 s^{-1}]
β thermal expansion coefficient [K^{-1}]
Δt time step [non dimensional]
δ_{ij} Kronecker delta
θ tangential coordinate
κ molecular conductivity [W m^{-1} °C^{-1}]
κ_t turbulent conductivity [W m^{-1} °C^{-1}]
μ dynamic viscosity [kg m^{-1} s^{-1}]
μ_t turbulent dynamic viscosity [kg m^{-1} s^{-1}]
v cinematic viscosity [m^2 s^{-1}]
ρ density [kg m^{-3}]
σ Froude number ($\sigma = Gr^*/Re^2$)
ϕ general function
ω rotation speed [s^{-1}]
∞ reference property.

Subscripts

$()_{ij}$ tensor notation
x_i Cartesian coordinate in i direction [non dimensional]
t turbulent property
s sub-grid scale property.

Acronym

LES large-eddy simulation.

1. Introduction

Natural convection heat transfer from horizontal cylinders placed in an infinite fluid medium has been studied

* Corresponding author

0017–9310/98/$—see front matter © 1998 Elsevier Science Ltd. All rights reserved
PII: S0017–9310(98)00153–7

extensively, both theoretically and experimentally. Many studies have been developed accounting only for the natural convection effects, where only the average heat transfer coefficients were obtained [1].

The literature on transient combined free and forced convection is relatively scarce. Sharman and Sukhatme [2] and Vilimpco et al. [3] studied the combined convection heat transfer from a heated tube in a transverse air stream and also in Newtonian liquids around the circular cylinder. A particular case of this problem is the combined convection around a rotating heated cylinder. This type of flow is of interest in many technological applications such as axis-bearing systems [4], rotating waste burners [5], cooling of rotating machinery, the design of rotating heat exchangers, the rotating heat pipe and the drying of paper [6]. One of the first studies in this area was realised by Dropkin and Carmi [7]. They concluded that the convection heat transfer coefficient is a function of three distinct regions: (a) the region where the buoyancy force determines the heat transfer coefficient and is independent of the rotation of the cylinder; (b) the region where both the buoyancy and the rotation are important and (c) the region where the convection heat transfer depends only on the rotation of the cylinder.

At low rotational speeds the flow has a behaviour like natural convection. As the rotation increases the heat transfer coefficient decreases until a minimum value is attained at a critical rotation speed. After this critical value it is found to increase with the increase of rotational speed and depends only on this parameter. Etemad [8] and Dropkin and Carmi [7] reported that this critical point can be defined at a Froude number $\sigma = Gr^*/Re^2 = 1$. On the other hand, Anderson and Saunders [9] argued, based on analytical results, that the transition point can be defined at $\sigma = 0.84$. Unfortunately, there is not enough information to confirm this point and hence there is not any conclusive answer to this question.

Sharman and Sukhatme [2] and Vilimpoc et al. [3] have studied the combined convection heat transfer process from a heated and rotating tube in a transverse air stream. They determined experimentally the average Nusselt number. Ball [6] studied, numerically and experimentally, the combined convection over a heated rotating cylinder. His numerical investigation is limited to small rotational speeds. Experimentally, he pointed out that, for higher rotational speed, the flow around the cylinder becomes three-dimensional and the associated physical instabilities may be responsible for the increase in the heat transfer coefficient.

Balparda et al. [10] developed a computational code based on the finite volume method with an UPWIND convective interpolation scheme with a precision of the first order. They obtained some interesting results, like the visualisation and the mean Nusselt number behaviour, as a function of the Reynolds number. Their results are limited by the high numerical diffusion generated by the UPWIND scheme.

In the present work a modified third order QUICK scheme [11] has been implemented in this code, in order to improve its performance. The Smagorinksy [12] subgrid scale turbulence model has been also implemented in this code, which characterises the large-eddy simulation. This code was used to study the combined convection over the horizontal heated rotating cylinder.

The first part of the work has been dedicated to the classical case of natural convection, without rotation. The numerical results were compared with experimental data and with other numerical results. The second part was dedicated to the configuration of combined convection over the rotating cylinder. The numerical results were compared with the experimental results of Ball [6]. Finally the code has been used to perform various simulations in order to obtain a correlation of the Nusselt number as a function of the Froude and Grashof numbers. The proposed correlation accounts for both the buoyancy and the rotation effects.

2. Governing equations

The transient combined convection over a horizontal, heated and rotating cylinder is governed by the continuity, the Navier–Stokes and the energy equations. The flow is considered incompressible with constant physical properties, except the density in the body force term, which is modelled using the Boussinesq approximation.

Turbulence is fundamentally a three-dimensional phenomenon. The present problem will be analysed with a two-dimensional approximation due to its transitional nature. As suggested by Ball [6] the three-dimensional instabilities appear because the cylinder rotation effects are more important compared with the buoyancy effects (the inverse of the Froude number). As will be shown, the results presented in the present work are limited to the operational regimes characterised by low rotation effects. In this situation two-dimensional LES is justified only by the physical specificity of this particular flow.

In large-eddy simulation, every variable f is decomposed in one part related to the large scale and another one related to the sub-grid scale:

$$f(\vec{x},t) = \bar{f}(\vec{x},t) + f'(\vec{x},t). \tag{1}$$

This scale separation is performed with the help of a filter G, defined as follows:

$$\bar{f}(\vec{x}) = \int_D G(\vec{x}-\vec{x}')f(\vec{x}')\,\mathrm{d}\vec{x}'. \tag{2}$$

Applying this filtering operation to the governing equations [14], the following equations are obtained:

$$\frac{\partial \vec{u}}{\partial t}+\nabla\cdot(\vec{u}\vec{u}) = -\frac{1}{\rho_\infty}\nabla\bar{p} + \beta(\bar{T}-T_\infty)\vec{g}+\nabla\cdot(v\nabla\vec{u}-\overline{\vec{u}'\vec{u}'}) \quad (3)$$

$$\frac{\partial \bar{T}}{\partial t}+\nabla\cdot(\vec{u}\bar{T}) = \nabla\cdot(\kappa\nabla\bar{T}-\overline{\vec{u}'T'}) \quad (4)$$

$$\nabla\cdot\vec{u} = 0. \quad (5)$$

The bar over the variables indicates the filtering operation; the term $\overline{\vec{u}'\vec{u}'}$ is the sub-grid Reynolds tensor and $\overline{\vec{u}'\bar{T}'}$ is the turbulent thermal energy flux. The Reynolds's tensor is modelled with the Boussinesq hypothesis:

$$-\overline{\vec{u}'\vec{u}'} = 2v_t\bar{S}_{ij}-\frac{2}{3}K_s\delta_{ij}, \quad (6)$$

where K_s is the sub-grid turbulent kinetic energy, δ_{ij} is the Kronecker delta and $\bar{S}_{ij}$ is the deformation rate, given by the following equation:

$$\bar{S}_{ij} = \frac{1}{2}\left(\frac{\partial\bar{u}_i}{\partial x_j}+\frac{\partial\bar{u}_j}{\partial x_i}\right). \quad (7)$$

These general equations are rewritten in two-dimensional cylindrical co-ordinates and the following non-dimensional equations are obtained [10], using v, R and ΔT for normalization:

$$\frac{\partial(r\bar{u})}{\partial r}+\frac{\partial\bar{v}}{\partial\theta} = 0 \quad (8)$$

$$\frac{\partial\bar{u}}{\partial t}+\frac{1}{r}\frac{\partial(r\bar{u}\,\bar{u})}{\partial r}+\frac{1}{r}\frac{\partial(\bar{v}\,\bar{u})}{\partial\theta}-\frac{\bar{v}^2}{r} = -\frac{\partial\bar{p}}{\partial r}+Gr^*\bar{T}\sin\theta+(1+v_t^*)\times\left[\frac{1}{r}\frac{\partial}{\partial r}\left(r\frac{\partial\bar{u}}{\partial r}\right)+\frac{1}{r^2}\frac{\partial}{\partial\theta}\left(\frac{\partial\bar{u}}{\partial\theta}\right)-\frac{2}{r^2}\frac{\partial\bar{v}}{\partial\theta}-\frac{\bar{u}}{r^2}\right] \quad (9)$$

$$\frac{\partial\bar{v}}{\partial t}+\frac{1}{r}\frac{\partial(r\bar{u}\,\bar{v})}{\partial r}+\frac{1}{r}\frac{\partial(\bar{v}\,\bar{v})}{\partial\theta}+\frac{(\bar{u}\,\bar{v})}{r} = -\frac{1}{r}\frac{\partial\bar{p}}{\partial\theta}+Gr^*\bar{T}\cos\theta+(1+v_t^*)\times\left[\frac{1}{r}\frac{\partial}{\partial r}\left(r\frac{\partial\bar{v}}{\partial r}\right)+\frac{1}{r^2}\frac{\partial}{\partial\theta}\left(\frac{\partial\bar{v}}{\partial\theta}\right)+\frac{2}{r^2}\frac{\partial\bar{u}}{\partial\theta}-\frac{\bar{v}}{r^2}\right] \quad (10)$$

$$\frac{\partial\bar{T}}{\partial t}+\frac{1}{r}\frac{\partial(r\bar{u}\bar{T})}{\partial r}+\frac{1}{r}\frac{\partial(\bar{v}\bar{T})}{\partial\theta} = \left(\frac{1}{Pr}+\frac{\alpha_t}{v}\right)\frac{1}{r}\frac{\partial}{\partial r}\left(r\frac{\partial\bar{T}}{\partial r}\right)+\frac{1}{r^2}\frac{\partial}{\partial\theta}\left(\frac{\partial\bar{T}}{\partial\theta}\right), \quad (11)$$

where $v_t^* = v_t/v$ is the dimensionless eddy viscosity. The diffusion terms were linearised while the physical properties are not considered as constants in the calculations. They are evaluated explicitly. The eddy viscosity v_t is calculated using the Smagorinsky model:

$$v_t = (C_S l)^2\sqrt{2\bar{S}_{ij}\bar{S}_{ij}}, \quad (12)$$

where C_S is the Smagorinsky constant. The characteristic length l is defined as:

$$l = \sqrt{r\Delta\theta\Delta r}. \quad (13)$$

The turbulent thermal diffusion α_t is calculated with the turbulent Prandtl number $v_t/\alpha_t = 0.6$ [15, 16]. In these equations, Pr is the Prandtl number, $Gr^* = g\beta R^4 q''/v^2\kappa$ is the Grashof number based on the heat flux q'' and the radius R. The reference parameters used to obtain the dimensionless equations are: v/R for the velocities, $\Delta T = q''R/\kappa$ for the temperature difference and R^2/v for time. With these definitions one can also obtain the following dimensionless parameter:

$$C_p = (p-p_\infty)/\left(\frac{\rho v^2}{R^2}\right),$$

as the pressure coefficient and $Re = \omega R^2/v$, as the Reynolds number, where ω is the angular speed of the cylinder. The Rayleigh number is defined as $Ra^* = Gr^*Pr$.

To establish the boundary conditions it is necessary to make some physical considerations. In the pure free convection, the flow is symmetric about a vertical plane containing the axis of the cylinder and the solution domain can be taken as a half of the flow field. In the rotating cylinder case this symmetry disappears and the solution domain must be complete. This is done by using an outer circular boundary. The radius of this domain is chosen as a function of the inverse of the Rayleigh number, as suggested by Qureshi and Ahmad [17]. In the present work the Rayleigh number ranges from 10^3 to 10^8 and the radius of the domain is taken as one-eighth of the cylinder radius.

This boundary is considered to be composed of an inflow part, where the radial velocity is negative ($u < 0$) and an outflow part, where the radial velocity is positive ($u > 0$) as suggested by Wang et al. [18]. In order to understand physically these boundary conditoins, the natural convection case is taken, where the flow comes from rest at infinity towards the cylinder and leaves the domain in a developed flow condition. In the case of the rotating cylinder, the boundary condition identification is more complex and is performed by identifying the sign of the radial velocity. Internally the cylinder is bounded by the solid surface, where a non-slip condition and an imposed heat flux condition are used. In order to have an adequate description of the flow near the wall there is a mesh refinement. The mesh size near the wall, in the radial direction is approximately 0.01 R. Any wall func-

tion has been used in this work. In this manner the following equations are established:

on the cylinder surface

$$u(R,\theta,t)=0;\quad v(R,\theta,t)=0;\quad -\frac{\partial T}{\partial r}(R,\theta,t)=1; \tag{14}$$

on the inflow and outflow regions

$$\frac{\partial u}{\partial r}(\infty,\theta,t)=0;\quad v(\infty,\theta,t)=0;\quad \frac{\partial T}{\partial r}(\infty,\theta,t)=0; \tag{15}$$

The governing equations subject to these boundary conditions are solved by using the following numerical method.

3. Numerical method

The finite-volume method proposed by Patankar [19], with staggered mesh, was recently considered with non-staggered mesh by Marchi et al. [20] and used by Balparda et al. [10]. The discretization volumes are illustrated in Fig. 1. A hybrid scheme is used for the time discretization: the velocity and the temperature are calculated explicitly and the pressure is calculated implicitly. The space discretization is performed with a third order QUICK scheme [21]. One can obtain the following expression for the generalised variable ϕ:

$$B_{p\phi}\phi_p^{n+1}=A_{p\phi}+L[p^{\phi}]^{n+1}\Delta V, \tag{16}$$

where

$$A_{p\phi}=\Sigma\left(a_{nb}\phi_{NB}^{n}\right)+B_{p\phi}\phi_p^{n}+L[S^{\phi}], \tag{17}$$

$$B_{p\phi}=\frac{\Delta V}{\Delta t}. \tag{18}$$

Here $L[\mathrm{p}^{\phi}]$ and $L[S^{\phi}]$ are the pressure and source terms in their integral forms; n is the previous time; $n+1$ is the current time; nb and NB are the neighbours values of the variable ϕ at the interfaces and centres of control volumes, respectively.

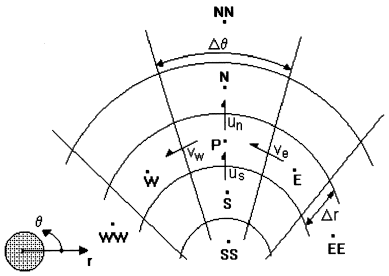

Fig. 1. Volume of discretization.

The linear system for the pressure is solved by a TDMA line by line method [19].

4. Numerical results

In this section the numerical results are presented. The calculations were performed in a cylindrical domain with an outer radius of 8 times the cylinder radius. This domain was discretized with a mesh of 112×30 points in the radial and tangential directions respectively. The mesh is regular in the tangential direction and grows progressively in the radial direction. A PC DX4 100 MHz was used and the CPU time, for each numerical experiment, was about 30 h.

4.1. Natural convection and statistical results

The QUICK interpolation scheme is third order precise but can provoke numerical instabilities [11]. These kinds of instabilities can be controlled by numerical artifices as proposed by March et al. [20]. It seems that it is also possible to achieve this control using a turbulence sub-grid scale model, which viscosity actuates in a similar fashion to the present calculation.

The time evolution of the natural convection is shown in Fig. 2(a)–(d). The temperature fields are visualised.

Numerical simulations were performed for various values of the Rayleigh number. The mean Nusselt numbers were obtained for two cases: without and with sub-grid scale model. We first present the results for the simulation without sub-grid scale model. Figure 3 shows the mean Nusselt number as a function of the Rayleigh number and the corresponding results due to Churchill and Chu [22] and Qurechi and Ahmad [17].

We see that for $Ra^{*}<10^{5}$ there is good agreement between the present prediction and the experimental and numerical results used for comparison. In this interval of operation regime the flow is laminar. On the other hand, for $Ra^{*}>10^{5}$ the flow begins to be transitional and the

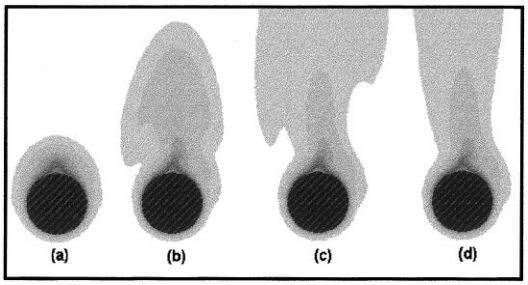

Fig. 2. Time evolution of the natural convection (the temperature fields); simulation with sub-grid scale model; $C_s=0.32$; $Ra^{*}=6.25\times10^{5}$; $Pr=0.7$; (a) $t=1$ s; (b) $t=2$ s; (c) $t=3$ s; (d) $t=4$ s.

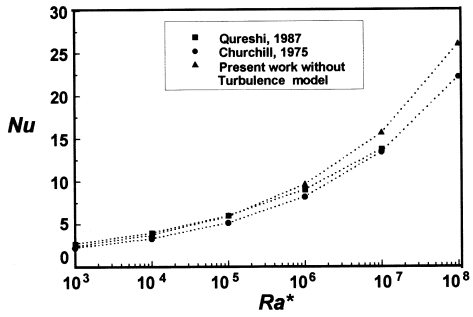

Fig. 3. Mean Nusselt number as a function of the Rayleigh number, without sub-grid scale model, $Pr = 0.7$.

effects due physical instabilities become important. The error for $Ra^* = 10^8$ can be up to 15%.

The results obtained with a sub-grid scale model (LES) are shown in Fig. 4 and the agreement with the available results for all values of the Rayleigh number is good. One also includes in this figure the result from Balparda et al. [10], obtained with a UPWIND first order interpolation scheme. It is interesting to observe that in this case (UPWIND) there is an artificial heat exchange augmentation due to the excess of numerical diffusion. We present in Fig. 5, the temperature profiles at $\theta = 90^\circ$C for the LES simulation (with QUICK scheme) and for the simulation with the UPWIND scheme. It is shown that the fluid, at this tangential position, is heated more in the LES simulation than in the UPWIND simulation. This is due to the spreading of the heated streak downwind of the cylinder, created by the numerical diffusion of the UPWIND scheme.

The tangential velocity component function of the radial position is presented in Fig. 6 for various values of the tangential coordinate. We see that at $\theta = \pm 90^\circ$C (vertical plane) this velocity component is zero due to the symmetry of the flow as shown in Fig. 7 by the mean temperature field and streamlines. At $\theta = 0^\circ$C this velocity component reaches its maximum as expected physically, for the pure natural convection. It is also shown that at $r/R = 4.5$ the temperature profile shows a behaviour corresponding to the boundary condition, equation (15). We notice that the limit of $r.R = 8$ used in the calculation is large enough to ensure a correct simulation.

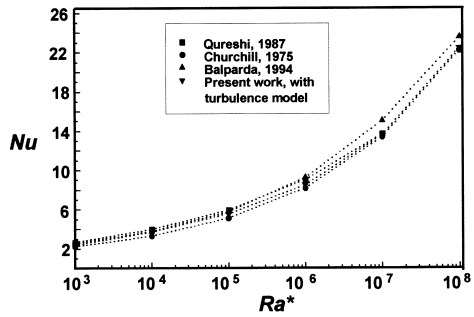

Fig. 4. Mean Nusselt number as a function of the Rayleigh number; large-eddy simulation; $C_s = 0.32$; $Ra^* = 1 \times 10^7$; $Pr = 0.7$.

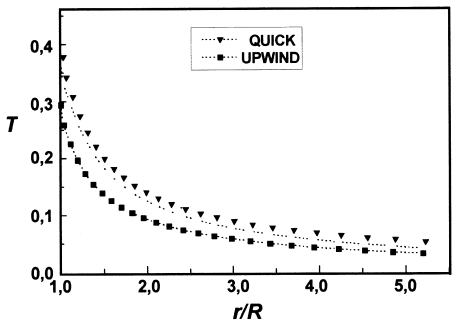

Fig. 5. Temperature distribution in the radial direction; UPWIND and QUICK interpolation scheme; $\theta = 90^\circ$C; $Ra^* = 1 \times 10^6$; $Pr = 0.7$; $C_s = 0.32$; calculations with QUICK scheme.

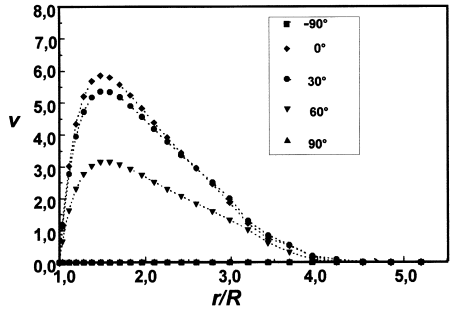

Fig. 6. Tangential velocity profiles; $Ra^* = 1 \times 10^3$; $Pr = 0.7$; $C_s = 0.32$.

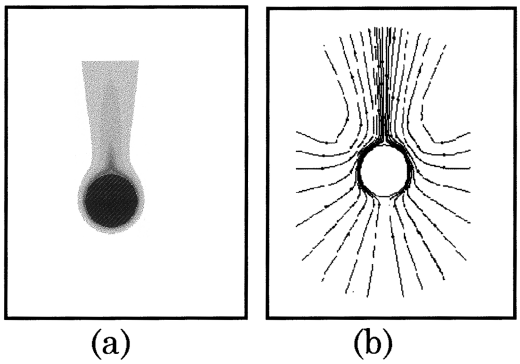

Fig. 7. Mean temperature fields (a) and streamlines (b); large-eddy simulation; $Ra^* = 1 \times 10^7$; $Pr = 0.7$; $C_s = 0.32$.

With these preliminary results for the classical case of pure natural convection we see that the method seems to be correct and consequently it will be used to simulate the more complex case of combined convection. The results are presented in the next section.

4.2. Large-eddy simulation of the combined convection

In this section the numerical results of the combined convection, for four values of the Rayleigh number are presented. The Froude number, defined as $\sigma = Gr^*/Re^2$, is a measure of the importance of the buoyancy or free-convection effects in relation to the inertia or forced convection effects. In the present work the forced convection is created by the rotation of the cylinder.

The following results are related to four values of the Froude number: $\sigma = \infty$; 2.0, 1.0 and 0.5. These values correspond respectively to 0, 52, 75 and 110 rpm. In all cases the Rayleigh umber is constant $Ra^* = 10^6$. Figure 8 shows the stationary flow regime for these four situations. The temperature fields are visualised. It can be observed that the flow is not symmetrical as in the previous case. The flow accelerates in the right-hand side of the cylinder, as shown in Fig. 9, where the effects of buoyancy and rotation are superimposed. Contrarily, at the left-hand side of the cylinder, the rotation effect is opposite to the buoyancy effect and hence the flow is slowed down, as shown in Fig. 10. Consequently the flow is distorted

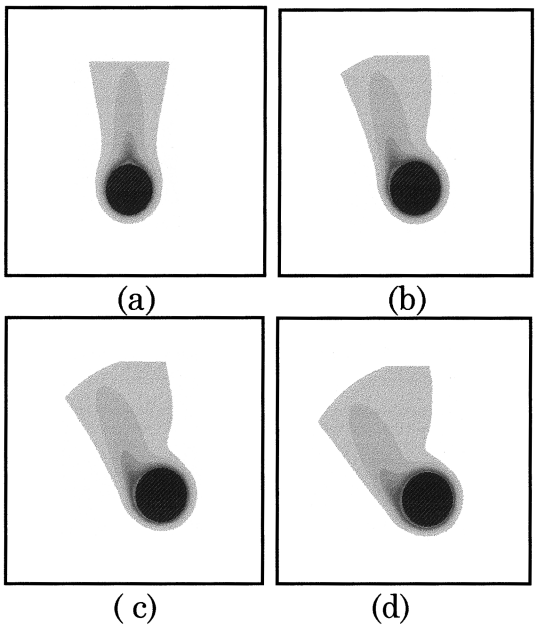

Fig. 8. Temperature fields over the rotating cylinder; $Ra^* = 1 \times 10^6$; $Pr = 0.7$; $C_s = 0.32$; (a) $Re = 0$, $\sigma = \infty$ (0 rpm); (b) $Re = 290$, $\sigma = 2$ (52 rpm); (c) $Re = 410$, $\sigma = 1$ (75 rpm); (d) $Re = 557$, $\sigma = 0.5$ (110 rpm).

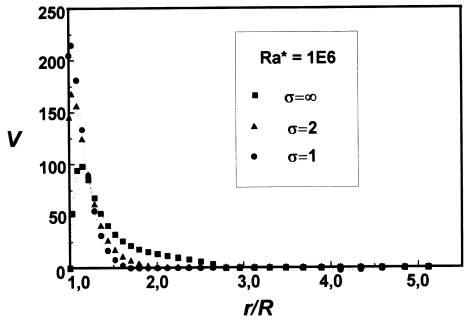

Fig. 9. Tangential velocity as a function of the radial position, for different values of σ, at $\theta = 0°C$; $Ra^* = 1 \times 10^6$; $Pr = 0.7$.

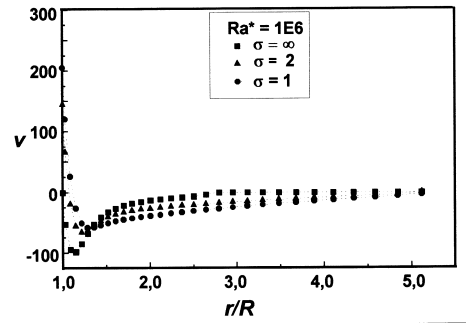

Fig. 10. Tangential velocity as a fuction of the radial position, for different values of σ, at $\theta = 180°C$; Ra* $= 1 \times 10^6$; $Pr = 0.7$.

towards the cylinder rotation sense (counter-clockwise). It is interesting to observe that even for the high rotation case, there is always a heated fluid stream rising up due to the buoyancy effects (Fig. 8(d)).

The heat transfer coefficient depends only on the natural convection (buoyancy effects) for small values of the rotational speed and depends only on the forced convection for high values of the rotational speed. Obviously, there is an intermediate regime in which the two effects are equally dominant.

To demonstrate this problem, Fig. 11 shows the streamlines close to the cylinder surface, for the three values of the rotational speed, 52, 110 and 360 rpm. The cylinder rotation traps the fluid particles which stay entrapped and form a fluid layer which rotates with the cylinder. It is clear from this figure that the thickness of this layer increases as the rotational speed increases. This layer creates an additional resistance to the convection heat transfer. In the present two-dimensional calculations this layer is stable, but in a three-dimensional analysis it can degenerate in turbulence by successive bifurcation, as in the case of two concentrically rotating cylinders, as will be explained later. Consequently one can expect to have three regimes of heat transfer in this system: the first is governed only by the buoyancy effect (natural

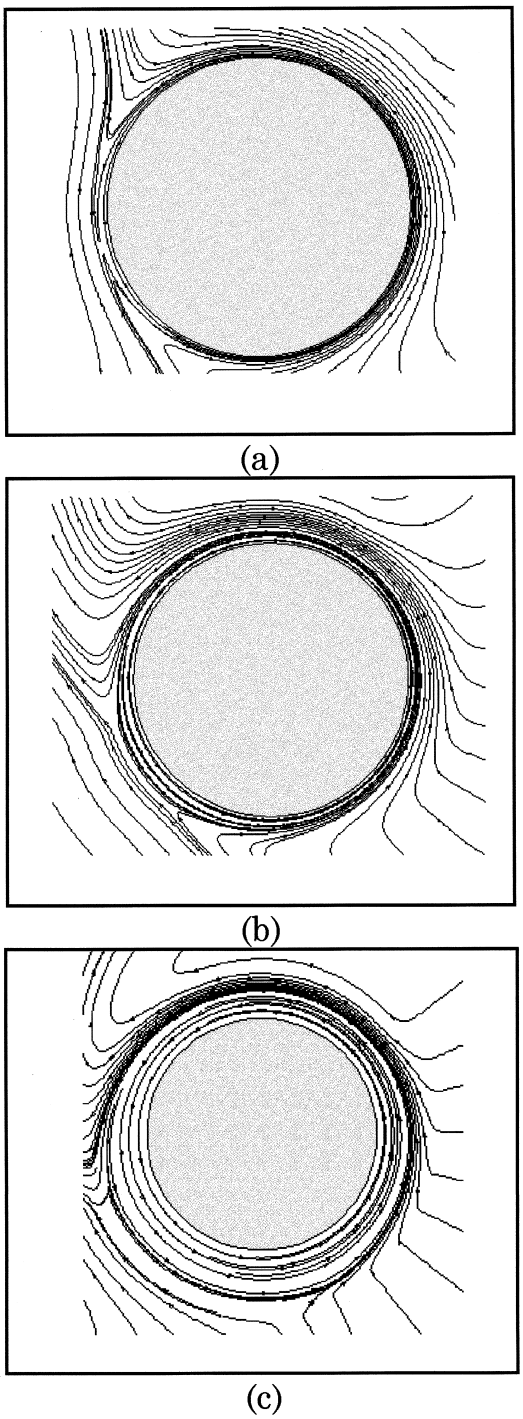

Fig. 11. Streamlines over the rotating cylinder; $Ra^* = 1 \times 10^6$; $Pr = 0.7$; $C_s = 0.32$; (a) $\sigma = 2$ (52 rpm); (b) $\sigma = 0.5$ (110 rpm); (c) $\sigma = 0.15$ (360 rpm).

convection); the second is governed by both the buoyancy and rotation effects (combined convection) and the third is governed only by the rotation effect (forced convection).

The local Nusselt umber is shown in Fig. 12 for four values of the Froude number. The Nusselt number distribution, for $\sigma = \infty$ (natural convection) is symmetrical about the vertical plane $\theta = \pm 90°C$. The minimum value is located at $\theta = 90°C$, the rear stagnation point (downwind stagnation point), where the diffusion heat transfer predominates over the convection effects. The maximum is located at $\theta = 270°C$ where the convection accelerates the heat transfer process.

As the process increases (Froude decreases) the point of minimum heat transfer displaces in the counter-clockwise sense. For $\sigma = 2$, for example, this point is $\theta \approx 170°C$. In reality it does not correspond to a stagnation point but represents a region of minimum velocity. Indeed, as indicated on Fig. 11, the distance between the streamlines in this region, is larger compared with the right-hand side of this figure. Consequently the minimum value of the Nusselt number is dislocated and this effect increases as the rotational speed increases. On the other hand the point of maximum Nusselt number decreases more than the minimum increases. Consequently the mean Nusselt number decreases with the rotational speed.

Figure 13 shows the mean Nusselt number (this mean value is calculated over the tangential coordinate θ as a function of $1/\sigma$ and Ra^*. The present numerical predictions are compared with the experimental results from Ball [6]. The agreement is good for the interval

$$0 < \frac{1}{\sigma} < \approx 1$$

(small rotational speeds). For

$$1 < \frac{1}{\sigma} < \infty$$

(high rotational speeds) the experimental results indicate

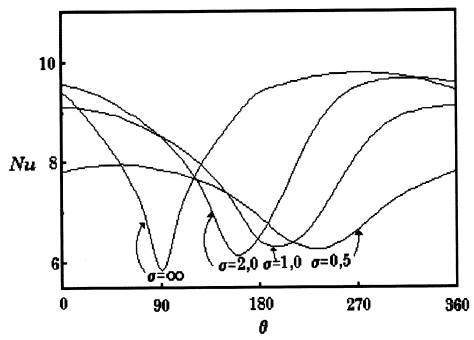

Fig. 12. Local Nusselt number as a function of the tangential position, for different values of σ; $Ra^* = 1 \times 10^6$; $Pr = 0.7$.

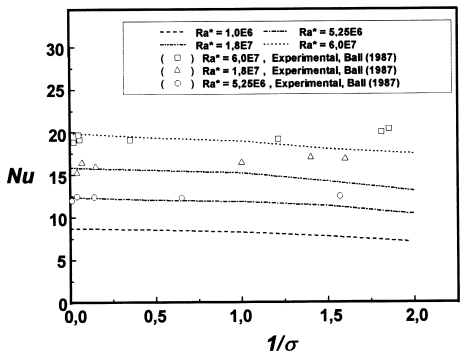

Fig. 13. The mean Nusselt number as a function of σ for different values of Ra^*; $Pr = 0.7$.

an increase of the Nusselt number as the rotation increases [6]. In contrast, the present numerical predictions show a decrease in the Nusselt number. This disagreement is basically due to the fact that the two-dimensional formulation is not adequate enough to simulate the three-dimensional nature of the flow pattern.

As the rotational speed increases, the thickness of the trapped layer (Fig. 11) increases and the flow near the cylinder becomes similar to the Couette flow between two rotating coaxial cylinders, as illustrated by Fig. 14(a). The transition of this flow to the turbulent regime is marked by the Taylor–Couette instabilities illustrated in Fig. 14(b). We suppose that these instabilities are very important to remove the inhibitive effect of this layer on the heat transfer process. The Taylor–Couette instabilities, being counter rotating, as indicated by Fig. 14(b), will transport hot fluid from the cylinder surface towards the external stream and cold fluid from the external stream towards the cylinder surface. This process creates a new mode of convection heat transfer and leads to an increase in the Nusselt number as the rotational speed increases. Consequently, a three-dimensional calculation must be done in order to simulate these instabilities and to obtain a more general Nusselt number correlation.

The above analysis indicates that the present numerical

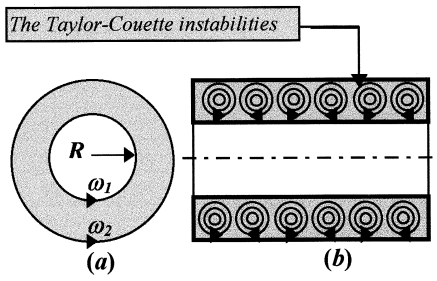

Fig. 14. Couette flow between two coaxial cylinders (a) and the Taylor–Couette instabilities (b).

results represent the physical problem at small rotational speeds as indicated earlier. Hence, a series of 44 numerical simulations were performed to obtain a correlation for the Nusselt number as a function of σ and Ra^*. Rayleigh number assumes the following values: 1.0×10^6, 5.25×10^6, 1.8×10^6 and 6.0×10^7. For each Rayleigh number, the inverse of the Froude number is equal to: 0.0, 0.2, 0.4, ..., 2.0 (step of 0.2). The Prandtl number is taken as being constant and equals 0.7. After some adjustment of the parameters the following correlation were obtained:

$$Nu = Nu_{NC} - 3.35\times10^{-8}\times Ra^*\times\sigma^{-0.783}, \tag{19}$$

where $1 \leqslant \sigma < \infty$ and $10^4 \leqslant Ra^* \leqslant 10^8$. The term Nu_{NC} is the Nusselt number for pure natural convection, given by the correlation proposed by Churchill et al. [22]:

$$Nu_{NC} = \left\{0.6+0.321x\left(\frac{Ra^*}{Nu_{NC}}\right)^{1/6}\right\}^2, \tag{20}$$

which is valid for $10^3 \leqslant Ra^* \leqslant 10^{12}$. The correlation proposed in the present work, equation (19), allows the evaluation of the heat transfer over a heated rotating cylinder and is valid within the indicated intervals. The error relative to the experimental results does not exceed 4%. It is important to observe that the difference between the results obtained using the two precedent correlations, equation (19) (combined convection) and equation (20) (natural convection) increases as Ra^* increases. For $Ra^* \approx 10^8$, for example, if the rotation effect is neglected, the error can reach 15%. This correlation is considered as the principal contribution of the present work.

5. Conclusions

The principal objective of the present work was to analyse and obtain the heat transfer correlation for a heated rotating horizontal cylinder, by large-eddy simulation. A two-dimensional code was developed using the finite-volume method with non-staggered grid technique. A third order QUICK interpolation scheme was used in combination with a sub-grid scale turbulence model.

The code was first tested in the classical configuration of natural convection giving good results. In sequence it was applied to analyse the situation of combined convection generated on a rotating heated cylinder. The predictions were found in good agreement with experimental results for small values of the rotational speed. A correlation for the heat transfer coefficient was proposed. Even when the rotational speed is small, the effect of this parameter is still important. Errors can reach 15% is rotation effects are neglected.

In order to obtain a more general correlation, three-dimensional calculations have to be done.

Acknowledgements

The authors are grateful to CNPq (Brazil) for financial support and to the post graduate course of Mechanical Engineering of the Federal University of Uberlândia for the scholarship.

References

[1] K. Sugiyama, Y. Ma, R. Ishiguro, Laminar natural convection heat transfer from a horizontal circular cylinder to liquid metals, Journal of Heat Transfer 113 (1991) 91–96.
[2] G.K. Sharma, S.P. Sukhatme, Combined free and forced convection heat transfer from a heated tube to a transverse air stream, Journal of Heat Transfer 91 (1959) 457–459.
[3] V. Vilimpoc, R. Cole, P.C. Sukanek, Heat transfer in Newtonian liquids around a circular cylinder, International Journal of Heat and Mass Transfer 33 (1990) 447–486.
[4] H. Heshmat, O. Pinkus, Mixing inlet temperature in hydrodynamic bearings, Journal of Tribology 108 (1986) 231–248.
[5] G.J. Menon, R.J. Silva, L.F. Rossi, R.M. e Francisco, Comportamento témico de fornos rotativos utilizados no co-processamento de resíduos industriais, XVI CILAMCE, Curitiba 1 (1995) 729–738.
[6] K.S. Ball, Mixed convection heat transfer in rotating systems, Ph.D. thesis, Drexel University, 1987.
[7] D. Dropkin, A. Carmi, Natural convection heat transfer from a horizontal cylinder rotating in air, Trans. ASME 79 (1957) 741–749.
[8] G.A. Etemad, Free convection heat transfer from a rotating horizontal cylinder to ambient air with interferometric study of flow, Trans. ASME 77 (1955) 1284–1289.
[9] J.T. Anderson, O.A. Saunders, Convection from an isolated heated horizontal cylinder rotating about its axis, Proc. Roy. Soc. London A217 (1953) 555–562.
[10] A. Balparda, A. Silveira Neto, M.A.V. Duarte, Numerical analysis of a two-dimensional natural and forced convection around a heated and rotating cylinder, Proceedings of Tenth International Heat Transfer Conference, Brighton, U.K. 1994.
[11] Y. Chen, R.A. Falconer, Advection–diffusion modelling using the modified QUICK scheme, International Journal for Numerical Methods in Fluids 15 (1992) 1171–1196.
[12] J. Smagorinsky, General circulation experiments with primitive equations, Monthly Weather Review 91 (1963) 99–164.
[13] R.E.M. Morales, Simulação de grandes escalas da convecção mista sobre um cilindro rotativo aquecido, Dissertação de Mestrado, Universidade Federal de Uberlândia-UFU, 1996.
[14] A. Silveira Neto, D. Grand, M. Lesieur, Simulation numérique Bidimensionalle d'un écoulement turbulent stratifié derriére une marche, International Journal of Heat and Mass Transfer 34 (1991) 1999–2011.
[15] A. Silveiro Neto, D. Grand, O. Metais, M. Lesieur, A numerical investigation of the coherent structures of turbulence behind a backward-facing step, International Journal of Fluids Mechanics 256 (1993) 1–25.
[16] M. Lesieur, Turbulence in Fluids, Kluwer Academic Publishers, 1990.
[17] Z.H. Qureshi, R. Ahmad, Natural convection from a uniform heat flux horizontal cylinder at moderate Rayleigh numbers, Numerical Heat Transfer 11 (1987) 199–212.
[18] P. Wang, R. Kahawha, D.L. Nguyen, Transient laminar natural convection from horizontal cylinders, International Journal of Heat and Mass Transfer 34 (1991) 1429–1442.
[19] S.V. Patankar, Numerical Heat Transfer and Fluid Flow, Hemisphere Publishing Corp., New York, 1980.
[20] C.H. Marchi, C.R. Maliska. A.L. Bortoli, The use of co-located variables in the solution of supersonic flows, Proceedings of Tenth Brazilian Congress of Mechanical Engineering, 1989, 1, pp. 157–160.
[21] T. Hayase, J.A.C. Humphrey, R. Grief, A consistently formulated QUICK scheme for fast and stable convergence using finite-volume iterative calculations procedures, Journal of Computational Physics 98 (1992) 108–118.
[22] S.W. Churchill, H.H.S. Chu, Correlating equations for laminar and turbulent free convection from a horizontal cylinder, International Journal of Heat and Mass Transfer 18 (1975) 1049–1053.